Chemical Engineering Journal 506 (2025) 159954

Contents lists available at ScienceDirect

Chemical Engineering Journal

journal homepage: www.elsevier.com/locate/cej

Porphyrin-Based Posolytes: A Novel Approach to Advancing Aqueous Organic Redox Flow Battery Technology

Jorge Montero, Williane da Silva Freitas *, Mattia Forchetta, Pierluca Galloni, Barbara Mecheri, Alessandra D'Epifanio *

Department of Chemical Sciences and Technologies, University of Rome Tor Vergata, Via Della Ricerca Scientifica, 00133 Rome, Italy

ARTICLE INFO

Keywords:
Energy storage
Aqueous redox flow batteries
Porphyrin-derived posolyte
Electrolyte optimization
Battery performance study

ABSTRACT

Aqueous organic redox flow batteries (AORFBs) hold great promise for large-scale energy storage, particularly in integrating renewable energy into the grid. However, their development is constrained by the scarcity of efficient posolytes. This study opens a new pathway for advancing AORFBs by unlocking the potential of porphyrins as active electrolytes. Despite their promise, the electrochemical stability of porphyrins in aqueous environments has been a critical challenge. To address this issue, we propose the porphyrin metalation with Zn to allow the redox reaction within the water potential window and the optimization of the electrolyte to enhance the durability of porphyrin in π-cations formed during oxidation. We introduce an efficient synthesis method for obtaining zinc porphyrin (ZnTPPS) and demonstrate that its stability and redox reversibility can be significantly improved in mildly acidic buffer solutions. When paired with 1,1′-bis(3-sulfonatopropyl)-viologen as the negolyte, the resulting AORFB achieved a stable capacity of approximately 500 $mAhL^{-1}$ over 100 cycles, with nearly 100 % coulombic efficiency, reflecting superior electrochemical performance. These findings position ZnTPPS as a novel and promising posolyte, paving the way for more efficient AORFB systems.

1. Introduction

Renewable energy systems are essential for reducing the carbon dioxide emissions associated with electricity generation [1–5]. However, the intermittent nature of sources such as solar and wind presents challenges for large-scale energy storage [6,7]. Redox flow batteries (RFBs), which store electroactive species in two separate tanks to decouple energy and power, are well-suited for grid-scale energy storage [8–16]. Traditional, first-generation RFBs primarily rely on transition metal-based electrolytes, such as vanadium, a relatively established technology [17–20]. However, their widespread use in large-scale storage is limited by issues, including the high cost and scarcity of active materials, corrosive and hazardous electrolytes, and the crossover of active species through the membrane [21,22].

Aqueous organic redox flow batteries (AORFBs) exploit the reversible redox reactions of organic and organometallic compounds, making them suitable candidates to address issues related to vanadium-based RFBs [23–28]. Organics-based active materials are derived from earth-abundant elements and are cost-effective, and their large size mitigates crossover issues [29]. Additionally, using water as a solvent avoids unsustainable and flammable organic solvents.

Many redox molecules, such as quinoids, flavin, alloxazine, phenazine, and viologen derivatives, have been extensively developed as negolytes [30]. The first reported organic active materials for aqueous RFBs were quinoids like 1,2-dihydrobenzoquinone-3,5-disulfonic acid (BQDS), 1,4-dihydrobenzoquinone-2-sulfonic acid (BQS), and anthraquinone-2,7-disulfonic acid (AQDS) [31,32]. However, to enhance the electrochemical performance of these quinoids, highly acidic H_2SO_4 solutions are required [33,34]. Viologen derivatives possess fast redox kinetics, high redox potential, water solubility, and excellent stability at neutral pH, attributed to trimethylammonium groups on the viologen core [35–37]. Due to these properties, they have been used as best-performing negolytes in neutral-based systems [26,38–40]. While significant progress has been made in developing stable and water-soluble anolytes for AORFBs, most catholytes' redox-active species are limited to ferrocene and 2,2,6,6-tetramethylpiperidine-1-oxyl (TEMPO) derivatives. These species are promising candidates for pH-neutral AORFBs, but their stability under operating conditions remains limited [36,41]. Compared to ferrocene, TEMPO offers a higher redox potential (~ 400 mV) for achieving high energy

* Corresponding authors.
E-mail addresses: williane.freitas@uniroma2.it (W. da Silva Freitas), alessandra.d.epifanio@uniroma2.it (A. D'Epifanio).

https://doi.org/10.1016/j.cej.2025.159954
Received 26 September 2024; Received in revised form 11 January 2025; Accepted 24 January 2025
Available online 25 January 2025

and power densities in RFB systems [42]. Despite these advantages, the charge-neutral nature of 4-hydroxy-TEMPO leads to crossover contamination, causing battery capacity decay. Molecular modifications, such as introducing a positively charged ammonium group, have been reported to improve the stability of TEMPO-derivative redox-active species [42,43]. However, the modified TEMPO mono-cations' chemical stability and crossover issues lead to poor cycling performance [44]. Investigating new cost-effective redox-active materials that meet high activity and performance durability is critical to developing AORFB systems.

Recently, few studies have reported the potential of porphyrinoids for application in non-aqueous organic RFBs [45–47]. The cost factor and scalability of porphyrin-based systems have significantly improved over time, primarily due to advancements in synthetic methodologies and the expanding applications of porphyrins across various fields. Historically, synthesizing porphyrins was expensive, limiting their widespread utilization. However, innovative approaches such as mechanochemical synthesis [48], continuous flow of reactants into the heated reactor [49], and the introduction of novel catalysts and one-pot synthesis methodologies have further optimized the synthesis of porphyrins, reducing costs and enhancing scalability [50,51]. Furthermore, the broader applicability of porphyrins in various fields has also contributed to their cost-effectiveness. Porphyrins have been successfully integrated into diverse applications, including catalysis [37,52,53], molecular electronics such as sensors [41,54], solar cells [36], and water-splitting [55]. Studies have shown that modifications in the porphyrin structure, such as introducing electron-donating groups or employing co-sensitization strategies, can significantly enhance power conversion efficiencies in dye-sensitized solar cells [56,57]. Such applications enhance the value of porphyrins and justify the investment in their synthesis as the demand for functional materials grows, reducing costs for their commercialization.

Porphyrins are promising candidates for active electrolytes in AORFBs due to their unique electrochemical properties and structural versatility. The main advantages of porphyrins in AORFBs include their high redox activity due to favorable electronic structure, tunable electrochemical properties, and potential for enhanced stability and capacity retention. The small HOMO-LUMO gaps in porphyrins allow for rapid electron transfer, which is essential for efficient energy storage and conversion in AORFBs [58]. This characteristic enables porphyrins to participate in multiple redox reactions, enhancing the overall energy density of the battery systems [59]. Additionally, porphyrins can be chemically modified to optimize their redox potentials, further improving their performance [47]. The ability to tailor their molecular structure allows for the development of porphyrins that can maintain structural integrity and redox activity over extended cycling, which is crucial for the longevity of AORFBs [60].

Another advantage is the inherent stability of porphyrins in aqueous environment. Studies have shown that porphyrins can maintain their structural integrity and redox activity over cycling, which is critical for the longevity of AORFBs [61]. However, their stability under operational conditions can be compromised by side reactions, leading to capacity fade. For instance, nucleophilic attacks on the porphyrin structure can result in degradation, and this loss of structural integrity can decrease the active species' effective concentration, thereby limiting the energy density of the AORFB [62]. Moreover, the degradation of porphyrins through nucleophilic attacks can also lead to the formation of by-products that may further complicate the electrochemical environment. These by-products can interfere with the redox processes, leading to increased polarization and reduced cycling stability of the battery [63].

The electrochemical stability of porphyrins is critical for maintaining long-term performance in AORFBs, and any degradation can result in capacity fading over time, which is a significant concern for practical applications [64]. This instability can be exacerbated by reactive species in the electrolyte, which may further degrade the porphyrin compounds. For example, in alkaline conditions, the nucleophilic nature of hydroxide ions can accelerate the degradation of porphyrins, leading to a more pronounced capacity fade [65].

Although previous reports demonstrated that stability could be enhanced by modifying the porphyrin structure [66], achieving a balance between high activity and stability remains challenging in developing porphyrin-based AORFBs. In particular, aggregating porphyrin molecules can reduce solubility and hinder their electrochemical performance [67]. This phenomenon is particularly problematic in aqueous environments, where the tendency for porphyrin molecules to aggregate can significantly decrease the effective concentration of active species, thereby limiting the energy density of the battery [64]. Furthermore, while modifications have been reported to increase the solubility of porphyrins to levels that could enhance their performance, such as pairing with conductive materials like Ketjen Black to improve functional solubility, these solutions may not fully mitigate the aggregation issue [45].

While porphyrins present several advantages as active electrolytes in AORFBs, including high redox activity and tunable properties, challenges such as aggregation, solubility, and electrochemical stability must be addressed to facilitate their practical implementation in energy storage technologies.

In this work, we explore functionalized porphyrins as a new path to obtain redox-active candidates for application in AORFB systems. We propose an effective approach to synthesize a water-soluble posolyte based on zinc tetraphenyl porphyrin tetrasulfonate (ZnTPPS) by exploiting the effect of the sulfonate groups to enhance the macrocycle solubility and the metalation with Zn to shift the potential of the redox reaction [68] within the water stability potential window.

The unique electronic configuration of Zn, which possesses a d_{10} electron configuration, contributes to its stability and favorable redox characteristics compared to other transition metals. Studies have demonstrated that Zn-porphyrins exhibit lower binding energies and reduced ligand-field stabilization compared to their counterparts with metals like cobalt (Co) or nickel (Ni) [69]. This property allows Zn-porphyrins to maintain their structural integrity and functionality under conditions that might destabilize other metalloporphyrins. Moreover, the electrochemical properties of Zn-porphyrins can be finely tuned through structural modifications, such as introducing electron-donating or electron-withdrawing substituents. This tunability allows for the design of porphyrins with specific redox potentials tailored for targeted applications in photochemistry and catalysis [70–75]. In contrast, other metals like cobalt (Co) may not provide the same level of tunability or stability, often leading to more complex redox behavior that can hinder their practical applications [70,76]. These characteristics make Zn-porphyrins a promising choice as a posolyte for AORFB applications.

Different aqueous solutions were investigated to optimize the performance of the ZnTPPS. Electrochemical tests in a half-cell configuration combined with spectroscopical analysis indicated superior electrochemical stability of the ZnTPPS in mildly acidic buffer solution (pH 4,6), which is ascribed to mitigation of both demetallation of the porphyrin center and formation of J-aggregates. Experiments with a rotating disk electrode showed fast kinetic and diffusion during oxidation of the ZnTPPS, and the permeability tests using a Nafion N212 membrane confirm the beneficial effect of using functionalized macrocycles for preventing the crossover phenomenon. ZnTPPS was paired with 1,1′-bis(3-sulfonatopropyl)-viologen (BSP-Vi) as negolyte [77] and tested in an AORFB single-cell. The battery tests showed promising performance in terms of open circuit voltage (~ 1,2 V), capacity retention over cycling, and coulombic efficiency (close to 100 %), highlighting the potential of the synthesized ZnTPPS as an alternative posolyte for energy storage in AORFBs.

2. Experimental section

2.1. Materials preparation

Toluene (ACS purity, 99.5 %), 1,3-propane sultone (98 %), acetic acid glacial (ACS purity, 100 %), ammonium acetate (>98 %), zinc acetate dihydrate (ACS grade, 99 %), methanol (absolute grade for analysis) and dichloromethane (HPLC grade) were purchased from Sigma-Aldrich except for 5, 10, 15, 20-(tetra-4-sulfonatophenyl) porphyrin tetraamonium which was acquired from Porphychem.

2.1.1. Preparation of the zinc (II) tetraphenyl porphyrin tetrasulfonate tetra ammonium (ZnTPPS)

1 g (0.99 mmol) of 5,10,15,20-(tetra-4-sulfonatophenyl) porphyrin tetra ammonium (H_2TPPS^{4-}) was stirred with 1.92 g of zinc acetate (10 mmol) in 200 mL of methanol at 65 °C. After 3 h, the reaction was cooled until room temperature was reached, and the solvent was removed by filtration under vacuum. The product was purified *via* precipitation by dissolving ZnTPPS in 20 mL of methanol and adding 200 153 mL of dichloromethane. A dark purple powder was obtained with a yield of 94 %

2.1.2. Preparation of 1,1′-bis(3-sulfonatopropyl)-viologen (BSP-Vi)

Synthesis was carried out according to our previous work [77]. Briefly, 726 mg of 4,4′- bipyridine and 1.12 g of propanesultone were refluxed in toluene for 3 h under a nitrogen (N_2) atmosphere. The resulting white precipitate was filtrated, rinsed with acetonitrile, and dried using a vacuum system. An 88 % BSP-Vi yield was obtained (1.63 g).

2.2. Materials Characterization

^{1}H NMR analysis was performed using an NMR spectrometer Bruker Avance, and the spectra were recorded at a 700 MHz resonance frequency in D_2O at a sample concentration of 1.0 mg mL^{-1}. UV–Vis was carried out to investigate the aging of the synthesized electrolytes, and the spectra were recorded using a Cary 50 Scan (Varian, Palo Alto, California, USA).

Electrochemical half-cell tests were performed using a rotating disk electrode (RDE) setup. A glassy carbon RDE (AFE6R2GCPT, Pine Research Instrumentation, area = 0.196 cm^2) was used as the working electrode. A platinum wire (Amel 805/SPG/12) was used as a counter electrode, with a saturated calomel electrode (SCE, Amel 303/SCG/12) used as a reference electrode. Measurements were acquired with a VMP3 Potentiostat (BioLogic Science Instruments) controlled by EC-Lab V10.18 software. The potential values for all electrochemical tests were converted from the SCE to the standard hydrogen electrode (SHE) scale.

Voltammetry tests were performed in two different aqueous electrolytes, using 1 mM ZnTPPS concentration. Before the electrochemical tests, N_2 gas was purged in the electrolyte for 20 min. The N_2 atmosphere was maintained over the electrolyte surface during the experiments. Cyclic voltammetry (CV) was carried out, either in ammonium chloride solution (0.5 M NH_4Cl), whose pH was adjusted to 7 by dropwise adding NH_4OH, or in acetic buffer solution (0.1 M, CH_3COOH/CH_3COONH_4, pH = 4.6), keeping the concentration of NH_4^+ as the same as TPPS counterion to mitigate the possible crossover effects. Linear sweep voltammetry (LSV) curves were recorded in the acetate buffer solution (0.1 M, pH = 4.6), from 0.5 to 1.0 V *vs*. SHE at a 10 mVs^{-1} scan rate and different electrode rotation speeds (400, 800, 1200, 1600, and 2000 rpm).

A permeability test was conducted in an H-cell (Fig. S1). Compartment A contained a solution of ZnTPPS (0.1 M) in the acetate buffer solution (0.1 M, pH = 4.6), which was used to fill the ZnTPPS-free compartment B. A Nafion N212 membrane separated compartments A and B. The variation in ZnTPPS concentration in compartment B was monitored using UV–Vis spectroscopy over one month.

AORFB tests were conducted at room temperature and in an argon atmosphere using a 0.1 M solution (10 mL) of the electroactive species, ZnTPPS and BSP-Vi, in the acetate buffer (0.1 M, pH = 4.6) as the supporting electrolyte. The cell was assembled by sandwiching a Nafion N212 membrane between two electrodes, each composed of three stacked carbon papers (Sigracet SGL 39AA), placed between two graphite plates with serpentine flow fields (Poco Graphite, Fuel Cell Technologies, Albuquerque, New Mexico, USA). Two Viton rubber gaskets were used to seal the cell with a 2.25 cm^2 active area. The carbon paper electrodes were pre-treated at 400 °C in an air atmosphere for 24 h, and the N212 membrane was pre-activated by immersion at 60 °C first in H_2O_2 (3.0 vol%) and then in 0.5 M H_2SO_4 aqueous solution (1 h each). The membranes were stored immersed in distilled water for 24 h.

The AORFB was assembled in a glove box with an argon atmosphere. Before testing, argon was purged into the posolyte and negolyte tanks for 8 h to eliminate residual oxygen in the solutions. A flow rate of 80 $mLmin^{-1}$ was set on both sides using diaphragm pumps (KNF, Trenton, NJ, USA). Electrochemical studies of the battery were performed by galvanostatic charge–discharge cycling using a multi-channel VMP3 Potentiostat (BioLogic Science Instruments) controlled by EC-Lab V1.18 software. The area-specific resistance (ASR) was measured through electrochemical impedance spectroscopy (EIS) at open circuit voltage (OCV), with data normalized by the geometric electrode area (2.25 cm^2). The battery was cycled at current densities of 24 $mAcm^{-2}$ (2C as C/rate), 12 $mAcm^{-2}$ (C), 6 $mAcm^{-2}$ (0.5 C), and 3 $mAcm^{-2}$ (0.25 C) with cut-off voltages of 1.5 V and 0.01 V. Electrochemical parameters, such as theoretical capacity, theoretical energy density, and coulombic efficiency, were calculated according to Eqs S1 to S3.

3. Results and Discussion

The synthesis of ZnTPPS was carried out by reaction of H_2TPPS^{4-} with zinc acetate in a methanol solution, as illustrated in Fig. 1. The complete metalation of H_2TPPS^{4-} was monitored by UV–Vis spectroscopy, showing that the reaction was completed after 3 h when only ZnTPPS signals could be observed (Fig. S2). The ^{1}H NMR spectra for the synthesized ZnTPPS (Fig. S3) showed proton resonances for the pyrrole (8.90 ppm), ortho phenyl (8.30 ppm, and meta phenyl (8.15 ppm). These data resemble previous ^{1}H NMR analyses reported in the literature [78] and differ from the resonance signals evidenced in the ^{1}H NMR spectra of the free base H_2TPPS^{4-} (~ 8.8 ppm for the pyrrole, 8.4 ppm for ortho phenyl, 7.8 ppm for meta phenyl, and 7.3 ppm for the *para*-phenyl proton resonance [78,79], indicating that the metalation of H_2TPPS^{4-} goes to completion. Furthermore, the remaining acetate salt, separated via precipitation by adding dichloromethane to the methanol solution, was effectively removed, as confirmed by ^{1}H NMR, showing only ZnTPPS signals.

Long-term stability tests (1 month) were carried out in aqueous solutions at different pH to optimize the electrolyte composition and assess the porphyrin's suitability for an AORFB application. ZnTPPS was dissolved in acetate buffer aqueous solution at pH 3.4, 4.6, and in the pH 7 (NH_4Cl/NH_4OH) supporting electrolyte, and UV–Vis spectra were acquired over time to evaluate the effect of aging. Fig. 2a–c show UV–Vis spectra of ZnTPPS acquired for fresh and one-month-aged solutions.

At all investigated pH values, the UV–Vis spectra of fresh solutions show an intense Soret band at 420 nm and two weak bands at 550 and 600 nm, ascribed as Q bands [80]. The UV–Vis spectrum of the more acidic solution significantly changed, as the intensity of the characteristic ZnTPPS bands strongly decreased, indicating the disappearance of the metalloporphyrin, and a new band at 650 nm attributed to the absorption of the H_4TPPS^{2-} appeared. At highly acidic pH (Fig. 2a), the porphyrins tend to form a π-cation radical, and a positive charge is delocalized over the entire conjugated system of the porphyrin rings [81,82]. This radical is a powerful electrophile that can react readily with nucleophiles such as water to give isoporphyrins [83].

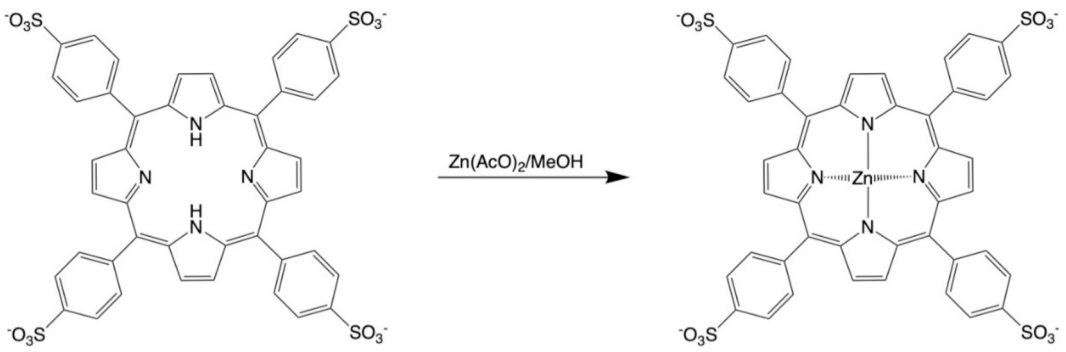

Fig. 1. Schematic for the H_2TPPS^{4-} (left) metalation with Zn to obtain ZnTPPs (right).

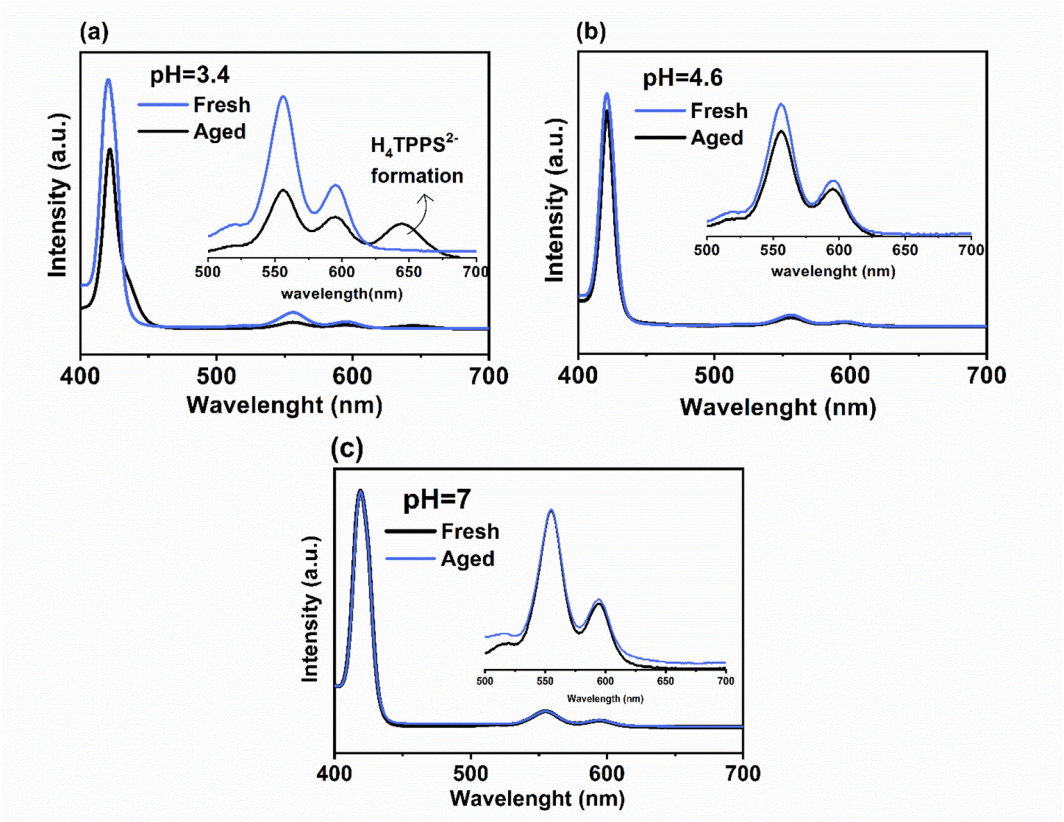

Fig. 2. UV–Vis spectra of ZnTPPS in acetate buffer solution at a pH of (a) 3.4, (b) 4.6, in the 0.1 M acetate buffer, and (c) pH 7 (0.1 M NH_4Cl/NH_4OH) for freshly prepared (blue) and a 1-month-aged (black) solution.

Furthermore, ZnTPPS undergoes demetallation by replacing Zn^{2+} with H^+ and forming the diacid H_4TPPS^{2+} (Fig. 2a); then, this diacid starts to form J-aggregates by π-π stacking interactions [84], illustrated in Fig. 3. The presence of the J-aggregates is evidenced by the appearance of new Soret and Q bands, observed at higher wavelength values (bathochromic shift or redshift), 430 and 645 nm, respectively [85,86]. These findings are aligned with the tendency of head-to-tail assembling of porphyrins with aromatic rings found at the *meso*-position of the porphyrin rings [87]. The formation of J-aggregates is also responsible for the solution color change from deep purple to turbid green, as shown in Fig. S4. In contrast, the UV–Vis spectrum of the ZnTPPS solution at pH 4.6 and 7 showed significantly less variation after aging, with no evidence of demetallation or J-aggregates formation even after one month. Notably, as the pH increases from 3.4 to 4.6 (Fig. 2b), the reduction in the absorbance of the Soret and Q bands becomes much less pronounced, and no aggregation-associated bands are observed. This inhibition of aggregate formation is even more evident at pH 7 (Fig. 2c), where the spectra before and after aging are almost identical. As a result, slightly acidic and neutral conditions were found to reduce J-aggregation, thereby increasing the lifetime of the porphyrin π-cations [88].

The effect of pH on J-aggregates formation is also confirmed by the CV analysis of the free-base porphyrin H_2TPPS^{4-} at pH 4.6 and 7 (Fig. S5). Within the potential window of 0.23 to 1.23 V *vs*. SHE, which is relevant for investigating potential posolytes for AORFB, Fig. S5 shows that an oxidation peak is observed at 1.13 V at pH = 7 due to the centered-ring one-electron oxidation of the H_2TPPS^{4-} into $H_2TPPS^{3-\bullet}$ [89]. However, this peak is not reversible. At pH 4.6, this oxidation peak is suppressed due to aggregation phenomena. At acidic pH, the nitrogen atoms of the central porphyrin macrocycle become protonated (pKa = 4.9) [90,91], facilitating the formation of J-aggregates. These aggregates form due to electrostatic interactions between the positively charged porphyrin cores and the negatively charged sulfonate groups on

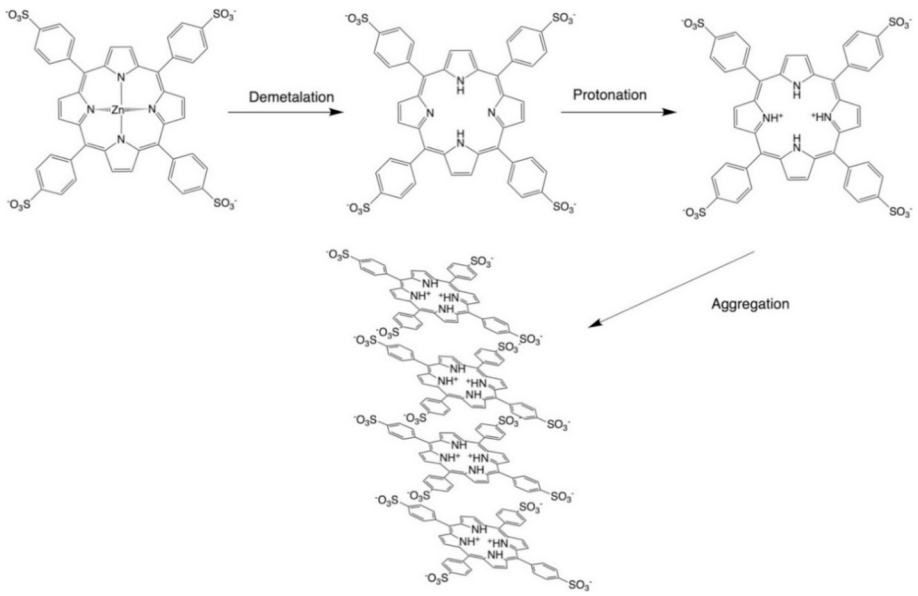

Fig. 3. Schematics for the ZnTPPS dementalization and aggregation process.

the molecule [92]. Conversely, at neutral to slightly basic pH levels, H_2TPPS^{4-} predominantly exists in its deprotonated form, which reduces aggregation. This behavior is attributed to the repulsive forces between the negatively charged sulfonate groups, which prevent the close packing necessary for aggregation [93]. The reversible redox process of H_2TPPS^{4-} lies beyond the water stability potential window, often necessitating organic solvents to prepare supporting electrolytes [86], making the free base unsuitable for an AORFB application.

A long-term cyclic voltammetry analysis was carried out to investigate the electrochemical stability of ZnTPPS at pH 4.6 and 7, at which no aging effects were observed from the UV–Vis analysis. As indicated in Fig. 4, upon metallation of the H_2TPPS^{4-} with Zn, a reversible redox process arising from the macrocycle ($ZnTPPS \rightleftharpoons ZnTPPS^{\bullet+} + e^-$) can be found within the water stability potential window, with a peak at 0.87 V *vs.* SHE for the ZnTPPS one-electron oxidation, and a peak at 0.80 V *vs.* SHE for the $ZnTPPS^{\bullet+}$ one-electron reduction. The presence of the metal changes the molecular orbitals of the porphyrin, reducing the HOMO-LUMO gap and decreasing the energy required for electron transfer [94,95]. Furthermore, the metallation of the H_2TPPS^{4-} with Zn(II) and Cu(II) relative to other transition metals such as Ni, Mn, Co, and Fe was found to mitigate the J-aggregation of a TPP-series of porphyrins in mildly acidic conditions with the disruption of the nanoassemblies by preventing possible stabilizing interactions between adjacent porphyrins [96,97]. The insertion of such metals in the porphyrin core was also found to benefit the porphyrin electrochemical stability since the metalloporphyrins containing Zn(II) and Cu(II) undergo only electrochemical reactions involving the π-ring system [98].

By comparing the CV in Fig. 4a and b, some differences are visible in the CV waves; at pH 4.6, the peaks are better defined, and the peak-to-peak separation is slightly lower, indicating that the overall process is kinetically favorable in acidic conditions. Interestingly, a slightly acidic environment also improved the stability of ZnTPPS compared to pH = 7, as indicated by a decrease of 8 % in the anodic peak current density after 700 CV cycles, concerning the 21 % in neutral conditions. The cathodic peak current density follows a similar trend, with a 2 % decrease at pH = 4.6 and 45 % at neutral pH. These findings can be ascribed to the higher stability of the $ZnTPPS^{+\bullet}$ monocation, formed upon the oxidation reaction ($ZnTPPS \rightleftharpoons ZnTPPS^{+\bullet} + e^-$) in a mildly acidic environment [88]. At pH = 4.0, it has been found that the ZnTPPS regeneration is promoted upon electroreduction, while at pH = 7, the $ZnTPPS^{+\bullet}$ can suffer further oxidation reactions, leading to degradation of the porphyrin rings [99,100] Since pH 4.6 was found to promote the electrochemical stability of ZnTPPS, mass transport, and kinetic parameters were investigated by performing LSV analysis in hydrodynamic conditions using an RDE.

The diffusion coefficient (*D*) of the active species is an essential

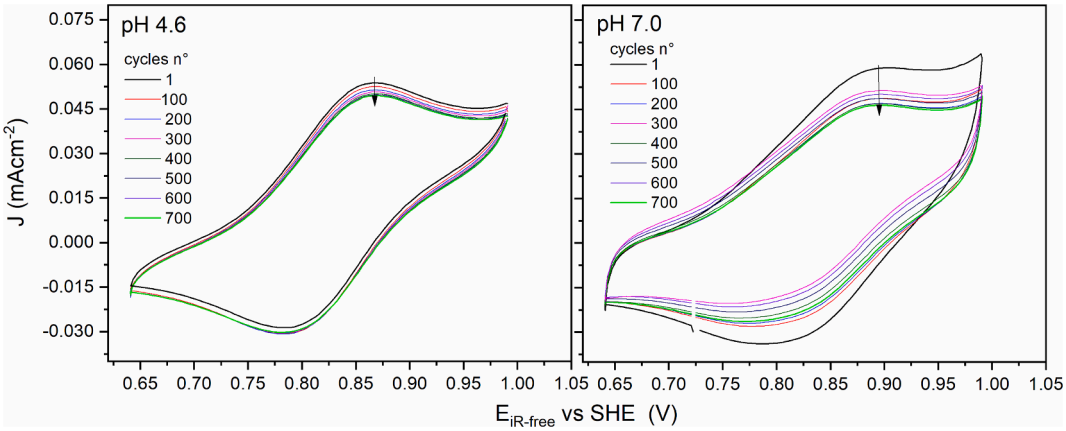

Fig. 4. CV at a 10 mVs^{-1} scan rate for 1 mM ZnTPPS in 0.1 M acetate buffer (pH = 4.6) and (b) 0.1 M NH_4Cl/NH_4OH (pH = 7) aqueous solutions.

parameter influencing RFB performance. Larger D values indicate a faster migration rate, promoting mass transfer kinetics of the electroactive species at the electrode surface and reducing the concentration polarization of the battery under a higher current density, which leads to a higher electrolyte utilization rate [101]. Another essential parameter to screening the activity of electroactive species for an RFB application consists of the standard kinetic rate constant (k^0), which indicates the kinetics facility of a redox couple [41,102]. D and k^0 were estimated by recording polarization curves at different rotation speeds (Fig. 5a). The LSV curves show a well-defined diffusion-limited current plateau for all investigated rotation speeds. To estimate the diffusion coefficient of the oxidized form of ZnTPPs, the Koutecký-Levich (K-L) theory was applied according to Eq. (1) [103,104]:

$$\frac{1}{J}=\frac{1}{J_k}+\left(\frac{1}{0.620nFD^{2/3}\nu^{-1/6}C}\right)\omega^{-1/2} \quad (1)$$

where J is the current density ($mAcm^{-2}$) at a specific overpotential, J_k is the kinetic current density ($mAcm^{-2}$), ω is the electrode rotation rate ($rads^{-1}$), C is the bulk concentration of ZnTPPS (1 mM), ν is the kinematic viscosity of acetate buffer solution (0.00753 $cm^2\,s^{-1}$), D is the diffusion coefficient ($cm^2\,s^{-1}$), F is the Faraday constant (96485 $Cmol^{-1}$), and n is the number of transferred electrons ($n = 1$).

Fig. 5b shows the K-L plot extrapolated to an infinite rotation rate to calculate the diffusion coefficient. The adopted current density values were sampled at the mass-transport-limited zone (E = 0.95 V) of the LSV curves recorded at the different rotation rates (Fig. 5a). The resulting D value estimated from the K-L analysis was 1.72×10^{-6} cm^2s^{-1}. Despite the larger size of ZnTPPs relative to traditional posolytes applied in aqueous and non-aqueous RFBs (Table S1), the obtained D value found for ZnTPPs reflects a good mass transfer capacity, critical to the RFB efficiency [105,106].

In addition, K-L analysis was also adopted to extrapolate the kinetic current density (J_k) for the ZnTPPS oxidation reaction (ZnTPPS ⇌ $ZnTPPS^{+\bullet} + e^-$) from the intercept of the K-L plot shown Fig. 5c. The current density values were sampled from 0.76 to 0.88 V, the potential range at which the reaction is limited mainly by kinetics. The obtained J_k values were used to draw the linear Tafel plot (Fig. 5d) and extrapolate the exchange current density (J_0) according to Eq. (2):

$$E = E^0+\frac{2.303RT}{\alpha_a F}\log J_0+\frac{2.303RT}{\alpha_a F}\log J_k \quad (2)$$

where E is the *i*R-corrected electrode potential, E^0 is 0.83 V, and α_a is the anodic transfer coefficient. From the Tafel analysis, the k^0 was determined by applying $J_0 = Fk^0C$, and for further comparison, it was also estimated by applying Nicholson's method, detailed in the Supplementary material (Eq. S4, Fig. S6).

According to the Tafel analysis, α_a and k^0 were found to be 0.55 and 8.42×10^{-2} cms^{-1}, respectively, and k^0 was comparable with that obtained by applying Nicholson's method ($k^0 = 9.20 \times 10^{-2}$ cms^{-1}), indicating a good agreement between both analysis. The calculated k^0 values point out relatively fast kinetics for the redox reaction, typical of quasi-reversible systems ($10^{-1} > k^0 > 10^{-5}$ cms^{-1}) in which both charge transfer and mass transport determine the current [107]. These findings are aligned with the non-zero intercept obtained from both Levich and K-L plots (Fig. 5b and S5), constructed using mass-transport-limited currents. A literature review shows that D and k^0 values are comparable to or exceed those observed for previously reported redox couples,

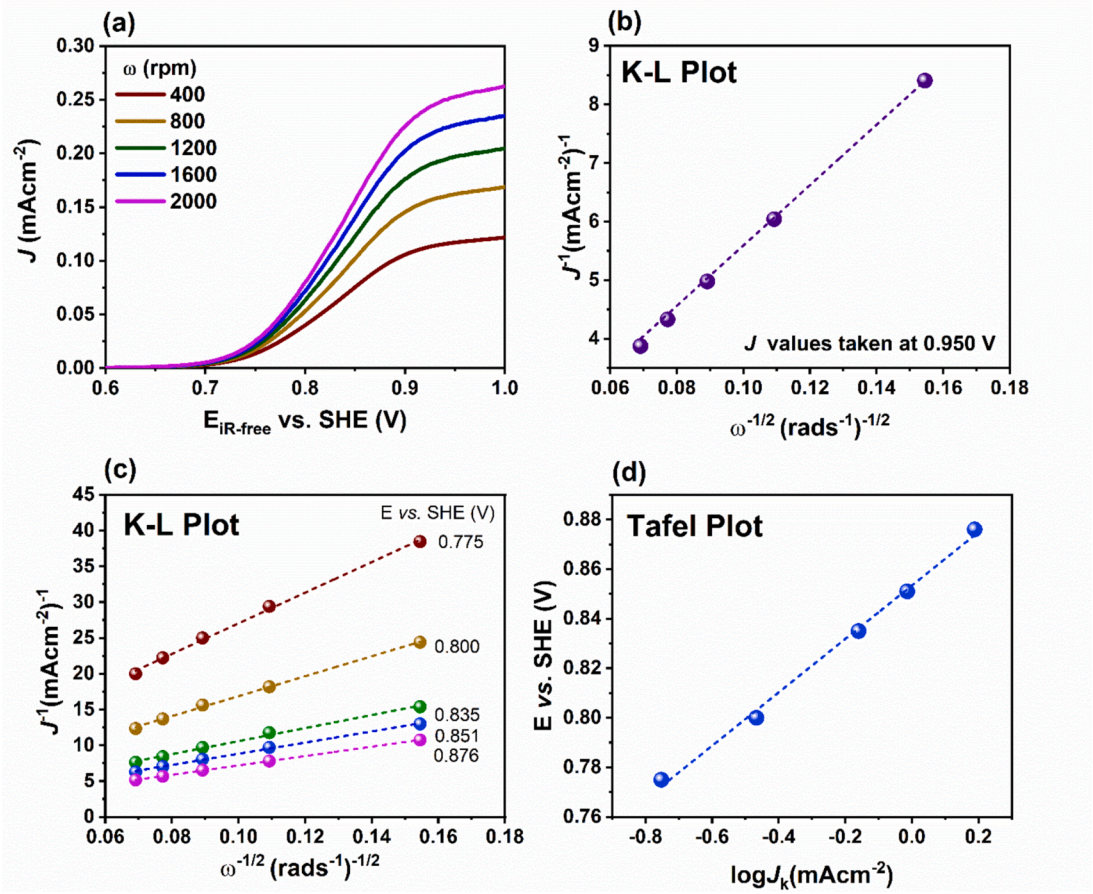

Fig. 5. (a) LSV curves at different rotation speeds and a 10 mVs^{-1} potential scan rate for the ZnTPPS (1 mM) in an acetate buffer aqueous electrolyte (0.1 M, pH = 4.6), (b-c) Koutecký-Levich (J^{-1} *vs.* $\omega^{-1/2}$) plots to extrapolation of the diffusion coefficient and the kinetic current density respectively, (d) Tafel plot adopted to the standard kinetic rate constant calculation.

including well-studied benchmarks such as ferrocene and TEMPO derivatives (Table S1), framing the ZnTPPs in the current literature as a promising posolyte for an aqueous RFB application.

Along with electrochemical parameters, other essential characteristics of a redox couple for AORFB applications are aqueous solubility and low permeability through the polymer membrane separator.

Since the solubility is one of the parameters providing an indication of the battery capacity and scalability constraints, we estimate the maximum amount of ZnTPPS that can dissolve in an aqueous environment, independently of aggregate formation or the resulting solution viscosity, by UV–Vis analysis as described in the supplementary material and shown in Fig. S7a.

A linear relation is observed from the plot of maximum absorbance for the Q band at 555 nm *versus* the ZnTPPS concentration (Fig. S7b). When the maximum solubility is reached, the absorbance value becomes constant since the highest concentration is achieved, with precipitation of the ZnTPPS excess. From this relation, the solubility of ZnTPPS in pH 4.6 acetate buffer solution was found to be 0.5 M.

Permeability tests were conducted in an H-shape cell, as described in the experimental section, to evaluate ZnTPPS crossover through the Nafion membrane. As illustrated in Fig. S8, no UV–Vis bands due to ZnTPPS were observed by UV–Vis spectroscopy, indicating the absence of crossover.

To test the viability of ZnTPPS as a catholyte for AORFBs, it was coupled with the 1,1′-bis(3-sulfonatopropyl)-viologen (BSP-Vi), a widely explored anolyte in RFB applications [77,108]. The AORFB based on the ZnTPPS/BSP-Vi couple has an expected open-circuit voltage (OCV) value of around 1.2 V (Fig. 6) and a maximum theoretical capacity of 13.4 AhL^{-1} when the maximum solubility is taken into account.

AORFB's electrochemical tests were performed with a 10 mL solution with 0.1 M electroactive species (ZnTPPS and BSP-Vi) in the acetate buffer supporting electrolyte (0.1 M, pH = 4.6) using a Nafion N212 membrane in this condition the theoretical capacity is estimated to be 2680 $mAhL^{-1}$.

Fig. 7a shows typical voltage charge and discharge profiles as a function of capacity; two different discharge plateaus are identified at 1.1 V and 0.2 V. The first plateau in Fig. 7a can be related to the reverse reaction of the charging process, i.e., BSP-Vi oxidation and ZnTPPS reduction. Regarding the second plateau at 0.2 V in the galvanostatic cycling, similar behavior has been reported for other planar molecules, such as $AQDSH_2$, due to the formation of dimers with their reduced species during the discharging process [109]. It is known that viologen-derivatives such as BSP-Vi are prone to form dimers with their π-radicals [110–113]. Despite this tendency, no plateau appearance at low voltage has been observed in previous studies dealing with the use of BSP-Vi as anolyte in AORFBs [114]. For this reason, the 0.2 V plateau likely comes from a ZTPPS's redox process. To investigate its nature, cyclic voltammograms were recorded at a broader voltage region for both BSP-Vi and ZnTPPS (Fig. S9); however, no further redox processes were indicated in the voltammograms. Since metalloporphyrins' dimerization was found to shift the oxidation reaction to lower voltages [115], CV of the ZnTPPS in a −0.8 to 1.1 V *vs.* SHE potential window, before and after the AORFB charge and discharge cyclic (Fig. S10) were also recorded. No remarkable changes were observed regarding peak-to-peak separation or reversible redox reactions between −0.8 and 0.4 V *vs.* SHE, which can be ascribed to the referred plateau. Only a current density decrease at the anodic (12.6 %) and cathodic (13.5 %) peak potential is observed and can be ascribed to the degradation of the π-cation ($ZnTPPS^{+\bullet}$) [88,100]. These current density decreases align with the stability test reported in Fig. 4a and are more pronounced due to the effects of a long-term test under the battery operating conditions. The reversible formation of porphyrin dimers is mostly identified at high concentrations of π-cations [116], which may explain the absence of corresponding low-voltage redox peaks in the postmortem CV measurements in the three-electrode cell setup, in contrast to the observed plateau during the battery discharge cycling.

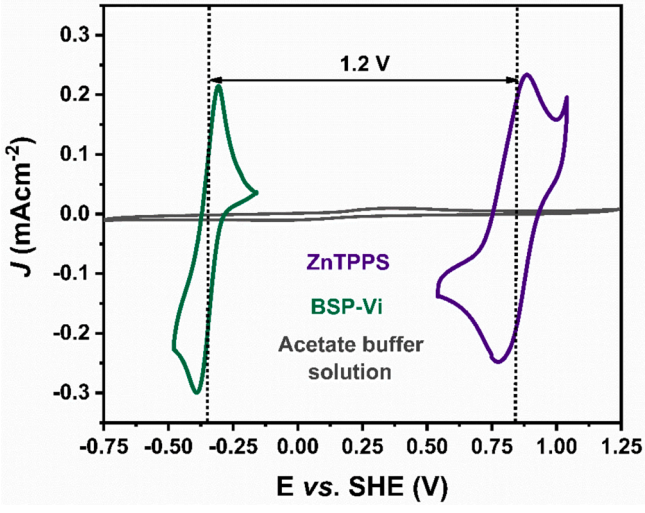

Fig. 6. CVs at a 10 mVs^{-1} scan rate for BSP-Vi ($E_{1/2}$ = -0.35 V) and ZnTPPS ($E_{1/2}$ = 0.83 V) in 0.1 M acetate buffer (pH = 4.6) aqueous electrolyte.

The current rate performance was investigated from 24 $mAcm^{-2}$ (2C) to 3 $mAcm^{-2}$ (C/4) (Fig. 7b); at higher current densities, 24 and 12 $mAcm^{-2}$, the Coulombic efficiency (CE) of the battery was nearly 100 % while decreased with decreasing current densities reaching 94 % at 6 $mAcm^{-2}$ and 88 % at 3 $mAcm^{-2}$. This finding can be attributed to a lack of stability of the porphyrin π-cation formed during the charging process, which remains in the solution for extended periods at lower current densities. To avoid this, the long-term galvanostatic cycling performance of the AORFB was evaluated at 12 $mAcm^{-2}$ (1C) (Fig. 7c). After an initial capacity decay between the 1st and 10th cycle, the RFB delivered a relatively high and stable capacity of around 500 $mAhL^{-1}$ over cycles, with a Coulombic efficiency of nearly 100 % and a 60 % capacity retention. Capacity was much higher than that achieved (~ 110 $mAhL^{-1}$) in our previous work for a neutral-pH AORFB assembled with ferrocene 1,1-disulfonic disodium salt (DS-Fc) as posolyte and BSP-Vi as negolyte [77], pointing out the performance improvement achieved with the ZnTPPS as compared to a ferrocene-derivative.

Fig. 7d shows the discharge polarization curve of the RFB recorded at 100 % state of charge. Before the polarization curve, the battery resistance value was measured as the high-frequency intercept with the x-axis of the Nyquist plot (Fig. S11), and a low area-specific resistance (ASR) of 2.95 Ωcm^2 was obtained, indicating a low contribution of the Nafion N212 membrane to the polarization ASR of the battery [117–120]. The *i*/V curve (Fig. 7d) shows a high open circuit voltage of around 1.2 V, a weak kinetic polarization (0.049 V drop at 5 $mAcm^{-2}$), and a relatively low ohmic resistance; these factors indicate both good electrodic activity and ion conduction in the Nafion N212 membrane. The voltage loss of the system seems to be affected predominantly by the mass transport of the species at high current density. Furthermore, a power density of 40.5 $mWcm^{-2}$ was registered.

To contextualize the performance of ZnTPPS as a posolyte in AORFBs, Table S2 summarizes the performance of AORFBs assembled with various redox couples reported in the literature. Table S2 compares performance metrics such as open-circuit voltage (OCV), maximum power density, theoretical capacity, capacity decay per cycle, and coulombic efficiency. This analysis highlights that our current results are consistent with the expected performance at this development stage. Due to the tunable properties of ZnTPPS, further performance enhancements can be achieved through targeted optimization efforts, primarily aimed at improving stability and reducing the overall costs of the final device. Introducing electron-donating groups (e.g., alkoxy groups) on the phenyl rings increases the electron density on the porphyrin core. This can stabilize the intermediate species produced during reactions and enhance electron transfer processes, improving

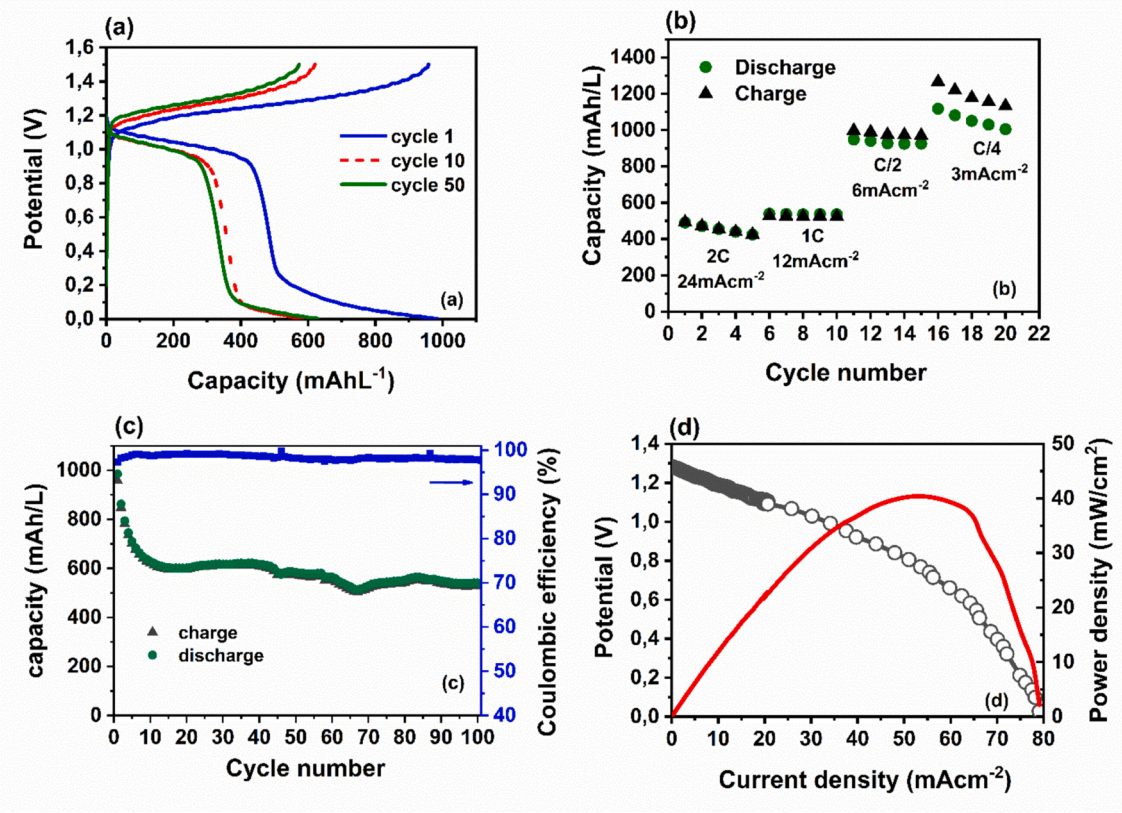

Fig. 7. Battery test for an AORFB cell assembled with the ZnTPPS posolyte and the BSP-Vi negolyte (10 mL, 0.1 M) in 4.6 pH acetate buffer solution. (a) voltage profiles for the 1, 10, and 50 cycles, (b) Battery charge–discharge capacity at different current densities, (c) charge–discharge capacity, and Coulombic efficiency versus cycle number at 12 $mAcm^{-2}$ (1C), and (d) polarization curve at a 100 % state of charge.

redox capabilities. Moreover, modulating the density of sulfonate ($-SO_3^-$) groups or using other water-solubilizing groups such as carboxyl (–COOH) or phosphate ($-PO_4^-$) may enhance the solubility and stability of the porphyrin under electrochemical cycling [72–75].

Regarding the cost-effectiveness of porphyrins as electroactive materials for AORFB applications, it is worth mentioning that the cost analysis of porphyrins synthesis is a multifaceted subject that encompasses various factors, including the choice of synthetic methods, the materials used, and the scalability of the processes. Commercially available metalloporphyrins are typically supplied in small quantities for research purposes, with prices varying based on the specific metal center, substituents, and purity. Table S3 shows that PorphyChem, Sigma-Aldrich, and other chemical suppliers offer a range of commercial metalloporphyrins, with different pricing information reflecting small-scale production. Scaling up production for industrial applications, such as in AORFBs, could lead to significant cost reductions due to economies of scale and process optimization.

4. Conclusions

A straightforward method was developed to synthesize a metal porphyrin complex as an aqueous redox-active posolyte based on zinc tetraphenyl porphyrin tetrasulfonate (ZnTPPS). Our study demonstrated the electrochemical stabilization of ZnTPPS in an aqueous environment using mild acidic buffer solutions (pH = 4.6), which enhanced the durability of the porphyrin π-cations formed during oxidation. Cyclic voltammetry tests revealed a 0.83 V *vs*. SHE redox potential, and Koutecký-Levich and Tafel analysis indicated fast kinetic ($k^0 = 8.42x10^{-2}$ cms^{-1}), and diffusion ($D = 1.72x10^{-6}$ cm^2s^{-1}) during the ZnTPPS oxidation. Moreover, no crossover was observed during the permeability test conducted in an H-cell, which is essential for applications in AORFB systems to ensure stability and efficiency. The newly developed porphyrin-based electrolyte was tested in an AORFB prototype, paired with 1,1′-bis(3-sulfonatopropyl)-viologen as the negolyte. After an initial capacity drop, galvanostatic cycling tests showed capacity retention of around 500 $mAhL^{-1}$ over 100 cycles, with a coulombic efficiency close to 100 %, indicating ZnTPPS as a promising posolyte candidate for AORFB applications.

This study proposes a novel approach to developing posolytes for AORFB systems, highlighting the use of porphyrinoids as a path to synthesize alternative redox couples with modulable chemical structures and able to meet activity and electrochemical durability while preventing the crossover through the polymeric membrane.

CRediT authorship contribution statement

Jorge Montero: Writing – original draft, Visualization, Methodology, Investigation, Formal analysis, Data curation, Conceptualization. **Williane da Silva Freitas:** Writing – review & editing, Writing – original draft, Visualization, Validation, Supervision, Methodology, Investigation, Formal analysis, Data curation, Conceptualization. **Mattia Forchetta:** Visualization, Methodology, Investigation, Formal analysis, Data curation. **Pierluca Galloni:** Writing – review & editing, Visualization, Validation, Supervision, Methodology, Investigation, Data curation, Conceptualization. **Barbara Mecheri:** Writing – review & editing, Visualization, Validation, Supervision, Resources, Methodology, Investigation, Funding acquisition, Formal analysis, Data curation, Conceptualization. **Alessandra D'Epifanio:** Writing – review & editing, Visualization, Validation, Supervision, Resources, Project administration, Methodology, Funding acquisition, Data curation, Conceptualization.

Declaration of competing interest

The authors declare that they have no known competing financial interests or personal relationships that could have appeared to influence the work reported in this paper.

Acknowledgments

This work has also received funding from the European Union – Next Generation EU in response to the MUR (Ministry of University and Research) call "PRIN (Project of National Interest) 2022": Project code: 202233PT4N. Authors also acknowledge financial support from "ORgANics for Green Electrochemical Energy Storage Project (ORANGEES)" funded by the Ministry of Environment and Energetic Security (*MASE*), Italy, PT 2019-2021, DD 27.10.2021 bando a, DD 05.08.2022.

Appendix A. Supplementary data

Supplementary data to this article can be found online at https://doi.org/10.1016/j.cej.2025.159954.

Data availability

Data will be made available on request.

References

[1] C. Liu, Z.G. Neale, G. Cao, Understanding electrochemical potentials of cathode materials in rechargeable batteries, Mater. Today. 19 (2016) 109–123, https://doi.org/10.1016/j.mattod.2015.10.009.
[2] W. da Silva Freitas, B. Mecheri, C. Lo Vecchio, I. Gatto, V. Baglio, V.C.A. Ficca, A. Patra, E. Placidi, A. D'Epifanio, Metal-organic-framework-derived electrocatalysts for alkaline polymer electrolyte fuel cells, J. Power Sources. 550 (2022) 232135, https://doi.org/10.1016/j.jpowsour.2022.232135.
[3] W. da Silva Freitas, D. Gemma, B. Mecheri, A. D'Epifanio, Air-breathing cathodes for microbial fuel cells based on iron-nitrogen-carbon electrocatalysts, Bioelectrochemistry. 146 (2022) 108103, https://doi.org/10.1016/j.bioelechem.2022.108103.
[4] W. da Silva Freitas, P.P. Machado Pico, A. D'Epifanio, B. Mecheri, Nanostructured Fe-N-C as bifunctional catalysts for oxygen reduction and hydrogen evolution, Catalysts. 11 (2021) 1525, https://doi.org/10.3390/catal11121525.
[5] B. Ricciardi, B. Mecheri, W. da Silva Freitas, V.C.A. Ficca, E. Placidi, I. Gatto, A. Carbone, A. Capasso, A. D'Epifanio, Porous iron-nitrogen-carbon electrocatalysts for anion exchange membrane fuel cells (AEMFC), ChemElectroChem. 202201115 (2023) 1–12, https://doi.org/10.1002/celc.202201115.
[6] J. Lopez, D.G. Mackanic, Designing polymers for advanced battery chemistries, Nat. Rev. Mater. 4 (2019) 312–330, https://doi.org/10.1038/s41578-019-0103-6.
[7] M. Duduta, B. Ho, V.C. Wood, P. Limthongkul, V.E. Brunini, W.C. Carter, Y. Chiang, Semi-solid lithium rechargeable flow battery, Adv. Energy Mater. 1 (2011) 511–516, https://doi.org/10.1002/aenm.201100152.
[8] Y. Zhen, C. Zhang, Y. Li, Imidazolium-functionalized liquid ferrocene derivative positive material enables robust cycling stability of non-aqueous redox flow battery, Chem. Eng. J. 468 (2023) 143697, https://doi.org/10.1016/j.cej.2023.143697.
[9] T. Sun, Y. Fan, X. Liu, J. Yang, J. Fu, Z. Tan, F. Chu, Battery performance promotion and mass transfer enhancement of organic redox flow battery by a novel spindle electrode design, Chem. Eng. J. 462 (2023) 142197, https://doi.org/10.1016/j.cej.2023.142197.
[10] N. Shi, G. Wang, Q. Wang, L. Wang, Q. Li, J. Yang, Acid doped branched poly (biphenyl pyridine) membranes for high temperature proton exchange membrane fuel cells and vanadium redox flow batteries, Chem. Eng. J. 489 (2024) 151121, https://doi.org/10.1016/j.cej.2024.151121.
[11] M.L. Perry, A.Z. Weber, Advanced redox-flow batteries: a perspective, Soc J Electrochem. 1 (2016) A5064–A5067, https://doi.org/10.1149/2.0101601jes.
[12] M. Daniel, N.P. Byron, C.M. Krowne, D. Curation, M. Daniel, I.M. Daniel, N. Byron, C.C. Krowne, M. Daniel, Harnessing redox flow batteries for industrial applications: opportunities and future directions, J. Power Sources. 591 (2024) 233889, https://doi.org/10.1016/j.jpowsour.2023.233889.
[13] D. Aaron, Z. Tang, A.Z. Alexander, B. Papandrew Thomas, Polarization curve analysis of all-vanadium redox flow batteries, J Appl Electrochem. 41 (2011) 1175–1182, https://doi.org/10.1007/s10800-011-0335-7.
[14] Z. Hou, X. Chen, J. Liu, Z. Huang, Y. Chen, M. Zhou, W. Liu, Towards a high efficiency and low-cost aqueous redox flow battery: a short review, J. Power Sources. 601 (2024) 234242, https://doi.org/10.1016/j.jpowsour.2024.234242.
[15] R.B. Jethwa, D. Hey, R.N. Kerber, A.D. Bond, D.S. Wright, C.P. Grey, Exploring the landscape of heterocyclic quinones for redox flow batteries, ACS Appl. Energy Mater. 7 (2024) 414–426, https://doi.org/10.1021/acsaem.3c02223.
[16] Á. Barros, E. Aranzabe, B. Artetxe, J.C. Duburg, L. Gubler, J.M. Gutiérrez-Zorrilla, U. Eletxigerra, Polyoxometalate-based symmetric redox flow batteries: performance in mild aqueous media, ACS Appl. Energy Mater. 7 (2024) 3729–3739, https://doi.org/10.1021/acsaem.4c00085.
[17] J. Paick, J.S. Yi, D. Lee, Detection and analysis of inner potential dynamics in vanadium redox flow batteries, Chem. Eng. J. 481 (2024) 148543, https://doi.org/10.1016/j.cej.2024.148543.
[18] Á. Cunha, J. Martins, N. Rodrigues, F.P. Brito, Vanadium redox flow batteries: a technology review, Int. J. Energy Res. 39 (2014) 889–918, https://doi.org/10.1002/er.
[19] J. Noack, N. Roznyatovskaya, T. Herr, P. Fischer, Die chemie der redox-flow-batterien angewandte, Angew. chem. 127 (2015) 9912–9947, https://doi.org/10.1002/ange.201410823.
[20] X. Xiao, D. Manaye, A. Mebreku, G. Chen, Y. Ou, Z. Huang, N. Hsu, H. Ku, Y. Wang, C. Wang, Defect-rich high-entropy spinel oxide catalyst for efficient vanadium redox flow battery, J. Power Sources. 597 (2024) 234178, https://doi.org/10.1016/j.jpowsour.2024.234178.
[21] J. Winsberg, T. Hagemann, T. Janoschka, M.D. Hager, U.S. Schubert, Redox-Flow-Batterien: von metallbasierten zu organischen Aktivmaterialien Angewandte, Angew.chem. 129 (2017) 702–729, https://doi.org/10.1002/ange.201604925.
[22] J. Montero, P. Navalpotro, A.D. Epifanio, B. Mecheri, S. Licoccia, J. Carretero-gonzález, Redox-active coordination polymers as bifunctional electrolytes in slurry-based aqueous batteries at neutral pH, J. Electroanal. Chem. 895 (2022) 115442, https://doi.org/10.1016/j.jelechem.2021.115442.
[23] L. Liu, X. Zhang, D. Zhang, K. Zhang, S. Hou, S. Wang, Y. Zhang, H. Peng, J. Liu, C. Yan, Regulating the N/B ratio to construct B, N co-doped carbon nanotubes on carbon felt for high-performance vanadium redox flow batteries, Chem. Eng. J. 473 (2023) 145454, https://doi.org/10.1016/j.cej.2023.145454.
[24] M. Shin, S. Park, K. Hyun, Y. Kwon, Spectroscopic and electrochemical analyses elucidating capacity degradation mechanism of iron-ligand complex and air in all iron aqueous redox flow batteries, Chem. Eng. J. 471 (2023) 144682, https://doi.org/10.1016/j.cej.2023.144682.
[25] W. Lee, K. In Shim, G. Park, J.W. Han, Y. Kwon, Rational design of composite supporting electrolyte required for achieving high performance aqueous organic redox flow battery, Chem. Eng. J. 464 (2023) 142661, https://doi.org/10.1016/j.cej.2023.142661.
[26] X. Lv, P. Sullivan, H. Fu, X. Hu, H. Liu, S. Jin, W. Li, D. Feng, Dextrosil-viologen: a robust and sustainable anolyte for aqueous organic redox flow batteries, ACS Energy Lett. 7 (2022) 2428–2434, https://doi.org/10.1021/acsenergylett.2c01198.
[27] M. Pan, W. Wang, H. Wang, J. Ma, M. Shao, Z. Jin, High-voltage and durable pH-neutral aqueous redox flow batteries based on quaternary ammonium cations functionalized naphthalene diimide and nitroxyl radical systems, J. Power Sources. 580 (2023) 233269, https://doi.org/10.1016/j.jpowsour.2023.233269.
[28] A. Ramar, F. Wang, R. Foeng, R. Hsing, Organic redox flow battery: are organic redox materials suited to aqueous solvents or organic solvents? J. Power Sources. 558 (2023) 232611 https://doi.org/10.1016/j.jpowsour.2022.232611.
[29] J. Asenjo-Pascual, I. Salmeron-Sanchez, P. Mauleón, M. Agirre, A.C. Lopes, O. Zugazua, E. Sánchez-Díez, J.R. Avilés-Moreno, P. Ocón, DFT calculation , a practical tool to predict the electrochemical behaviour of organic electrolytes in aqueous redox flow batteries, J. Power Sources. 564 (2023) 232817, https://doi.org/10.1016/j.jpowsour.2023.232817.
[30] D.G. Kwabi, Y. Ji, M.J. Aziz, Electrolyte lifetime in aqueous organic redox flow batteries: a critical review, Chem. Rev. 120 (2020) 6467–6489, https://doi.org/10.1021/acs.chemrev.9b00599.
[31] F.G. Mutti, T. Knaus, N.S. Scrutton, M. Breuer, N.J. Turner, Conversion of alcohols to enantiopure amines through dual-enzyme hydrogen-borrowing cascades, Science (80-.). 349 (2015) 1525–1529. https://doi.org/10.1126/science.aac9283.
[32] M.R. Gerhardt, C.J. Galvin, B. Huskinson, M.P. Marshak, C. Suh, X. Chen, A metal-free organic-inorganic aqueous flow battery, Nature. 505 (2014) 195–198, https://doi.org/10.1038/nature12909.
[33] T. Liu, X. Wei, Z. Nie, V. Sprenkle, W. Wang, A total organic aqueous redox flow battery employing a low cost and sustainable methyl viologen anolyte and 4-HO-TEMPO catholyte, Adv. Energy Mater. 6 (2016), https://doi.org/10.1002/aenm.201501449.
[34] M.R. Gerhardt, L. Tong, R. Gómez-bombarelli, Q. Chen, M.P. Marshak, C. J. Galvin, A. Aspuru-guzik, R.G. Gordon, M.J. Aziz, Anthraquinone Derivatives in Aqueous Flow Batteries, 1601488, Adv. Energy Mater. 7 (2017), https://doi.org/10.1002/aenm.201601488.
[35] J. Yu, M. Salla, H. Zhang, Y. Ji, F. Zhang, M. Zhou, Q. Wang, A robust anionic sulfonated ferrocene derivative for pH-neutral aqueous flow battery, Energy Storage Mater. 29 (2020) 216–222, https://doi.org/10.1016/j.ensm.2020.04.020.
[36] S. Hu, L. Wang, X. Yuan, Z. Xiang, M. Huang, P. Luo, Y. Liu, Z. Fu, Z. Liang, Viologen-decorated TEMPO for neutral aqueous organic redox flow batteries, Energy Mater. Adv. 2021 (2021) 1–8.
[37] K. Qu, Y. Liu, D. Hong, Z. Shen, X. Zhang, X. Han, A highly soluble and readily accessible viologen negolyte for pH-neutral aqueous organic redox flow batteries, J. Power Sources. 599 (2024) 234222, https://doi.org/10.1016/j.jpowsour.2024.234222.
[38] S. Jin, E.M. Fell, L. Vina-Lopez, Y. Jing, P.W. Michalak, R.G. Gordon, M.J. Aziz, Near neutral ph redox flow battery with low permeability and long-lifetime

phosphonated viologen active species, Adv. Energy Mater. 10 (2020) 1–10, https://doi.org/10.1002/aenm.202000100.
[39] M. Hu, W. Wu, J. Luo, T.L. Liu, Desymmetrization of viologen anolytes empowering energy dense, ultra stable flow batteries toward long-duration energy storage, Adv. Energy Mater. 12 (2022) 1–8, https://doi.org/10.1002/aenm.202202085.
[40] M. Pan, L. Gao, J. Liang, P. Zhang, S. Lu, Y. Lu, J. Ma, Z. Jin, Reversible redox chemistry in pyrrolidinium-based TEMPO radical and extended viologen for high-voltage and long-life aqueous redox flow batteries, Adv. Energy Mater. 12 (2022) 1–8, https://doi.org/10.1002/aenm.202103478.
[41] E.S. Beh, D. De Porcellinis, R.L. Gracia, K.T. Xia, R.G. Gordon, M.J. Aziz, A neutral pH aqueous organic- organometallic redox flow battery with extremely high capacity retention, ACS Energy Lett. 2 (2017) 639–644, https://doi.org/10.1021/acsenergylett.7b00019.
[42] B. Hu, M. Hu, J. Luo, T.L. Liu, A. Stable, Low permeable TEMPO catholyte for aqueous total organic redox flow batteries, Adv. Energy Mater. 12 (2022) 1–5, https://doi.org/10.1002/aenm.202102577.
[43] T. Janoschka, N. Martin, M.D. Hager, U.S. Schubert, An aqueous redox-flow battery with high capacity and power: the TEMPTMA/MV system, Angew. Chemie Int. Ed. 55 (2016) 14427–14430, https://doi.org/10.1002/anie.201606472.
[44] M. Li, S.A. Odom, A.R. Pancoast, L.A. Robertson, T.P. Vaid, G. Agarwal, H. A. Doan, Y. Wang, T.M. Suduwella, S.R. Bheemireddy, R.H. Ewoldt, R.S. Assary, L. Zhang, M.S. Sigman, S.D. Minteer, Experimental protocols for studying organic non-aqueous redox flow batteries, ACS Energy Lett. 6 (2021) 3932–3943, https://doi.org/10.1021/acsenergylett.1c01675.
[45] X. Wang, J. Chai, J. "Jimmy" Jiang, Redox flow batteries based on insoluble redox-active materials. A review, Nano Mater. Sci. 3 (2021) 17–24, https://doi.org/10.1016/j.nanoms.2020.06.003.
[46] T. Ma, Z. Pan, L. Miao, C. Chen, M. Han, Z. Shang, J. Chen, Porphyrin-based symmetric redox-flow batteries towards cold-climate energy storage, Angew. Chemie Int. Ed. 57 (2018) 3158–3162, https://doi.org/10.1002/anie.201713423.
[47] N.H. Mitchell, N. Elgrishi, Investigation of Iron(III) tetraphenylporphyrin as a redox flow battery anolyte: unexpected side reactivity with the electrolyte, J. Phys. Chem. c. 127 (2023) 10938–10946, https://doi.org/10.1021/acs.jpcc.3c01763.
[48] Q. Su, T.D. Hamilton, Extending mechanochemical porphyrin synthesis to bulkier aromatics: tetramesitylporphyrin, Beilstein J. Org. Chem. 15 (2019) 1149–1153, https://doi.org/10.3762/bjoc.15.111.
[49] P.B. Momo, B.S. Bellete, T.J. Brocksom, R.O.M.A. De Souza, K.T. De Oliveira, Exploiting novel process windows for the synthesis of meso-substituted porphyrins under continuous flow conditions, RSC Adv. 5 (2015) 84350–84355, https://doi.org/10.1039/c5ra16962c.
[50] B.Q. Li, S.Y. Zhang, X. Chen, C.Y. Chen, Z.J. Xia, Q. Zhang, One-Pot synthesis of framework porphyrin materials and their applications in bifunctional oxygen electrocatalysis, Adv. Funct. Mater. 29 (2019) 1–8, https://doi.org/10.1002/adfm.201901301.
[51] M.J.F. Calvete, L.D. Dias, C.A. Henriques, S.M.A. Pinto, R.M.B. Carrilho, M. M. Pereira, A cost-efficient method for unsymmetrical Meso-aryl porphyrin synthesis using NaY zeolite as an inorganic acid catalyst, Molecules. 22 (2017) 1–11, https://doi.org/10.3390/molecules22050741.
[52] V. Singh, S. Kim, J. Kang, H.R. Byon, Aqueous organic redox flow batteries, Nano Res. 12 (2019) 1988–2001, https://doi.org/10.1007/s12274-019-2355-2.
[53] X. Bai, Z. Su, J. Wei, L. Ma, S. Duan, N. Wang, X. Zhang, J. Li, Zinc(II)porphyrin-based porous ionic polymers (PIPs) as multifunctional heterogeneous catalysts for the conversion of CO2to cyclic carbonates, Ind. Eng. Chem. Res. 61 (2022) 5093–5102, https://doi.org/10.1021/acs.iecr.2c00161.
[54] S. Nasri, M. Guergueb, J. Brahmi, Y.O. Al-Ghamdi, F. Loiseau, H. Nasri, Synthesis of a novel Zinc(II) porphyrin complex, halide ion reception, catalytic degradation of dyes, and optoelectronic application, Crystals. 13 (2023), https://doi.org/10.3390/cryst13020238.
[55] F. Kuttassery, S. Sagawa, S. Mathew, Y. Nabetani, A. Iwase, A. Kudo, H. Tachibana, H. Inoue, Water splitting on aluminum porphyrins to form hydrogen and hydrogen peroxide by one photon of visible light, ACS Appl Energy Mater. (2019) 8045–8051, https://doi.org/10.1021/acsaem.9b01552.
[56] S. Mathew, A. Yella, P. Gao, R. Humphry-Baker, B.F.E. Curchod, N. Ashari-Astani, I. Tavernelli, U. Rothlisberger, M.K. Nazeeruddin, M. Grätzel, Dye-sensitized solar cells with 13% efficiency achieved through the molecular engineering of porphyrin sensitizers, Nat. Chem. 6 (2014) 242–247, https://doi.org/10.1038/nchem.1861.
[57] J.M. Ji, H. Zhou, Y.K. Eom, C.H. Kim, H.K. Kim, 14.2% Efficiency dye-sensitized solar cells by Co-sensitizing novel thieno[3,2-b]indole-Based organic dyes with a promising porphyrin sensitizer, Adv. Energy Mater. 10 (2020) 1–12, https://doi.org/10.1002/aenm.202000124.
[58] X. Peng, B. Ren, C. Sun, Y. Liao, F. He, T. Li, X. Sun, Z. Chen, W. Liu, P. Gao, Ultra-long lifespan ni based porphyrin complex cathode for organic alkali metal batteries, Batter. Supercaps. 7 (2024) 1–9, https://doi.org/10.1002/batt.202400031.
[59] Z. Rhodes, J.R. Cabrera-Pardo, M. Li, S.D. Minteer, Electrochemical advances in non-aqueous redox flow batteries, Isr. J. Chem. 61 (2021) 101–112, https://doi.org/10.1002/ijch.202000049.
[60] B. Ambrose, A. Kannan, M. Kathiresan, Evaluation of negolyte properties of supramolecular binary complexes based on viologen-cucurbit[7]urils, New J. Chem. 46 (2022) 5606–5613, https://doi.org/10.1039/d1nj05816a.
[61] M. Mansha, A. Ayub, I.A. Khan, S. Ali, A.S. Alzahrani, M. Khan, M. Arshad, A. Rauf, S. Akram Khan, Recent development of electrolytes for aqueous organic redox flow batteries (aorfbs): current status, challenges, and prospects, e202300284, Chem. Rec. 24 (2024), https://doi.org/10.1002/tcr.202300284.
[62] Y. Liu, P. Zhang, Z. Wu, G. Ding, X. Song, J. Ma, W. Wang, X.Z. Wang, Z. Jin, Biomimetic naphthoquinone zwitterion derivative with water-solubilizing amino acid side chain for high-stability aqueous redox flow batteries, ACS Energy Lett. 9 (2024) 586–593, https://doi.org/10.1021/acsenergylett.3c02530.
[63] S. Lv, J. Yuan, Z. Chen, P. Gao, H. Shu, X. Yang, E. Liu, S. Tan, M. Ruben, Z. Zhao-Karger, M. Fichtner, Copper porphyrin as a stable cathode for high-performance rechargeable potassium organic batteries, ChemSusChem. 13 (2020) 2286–2294, https://doi.org/10.1002/cssc.202000425.
[64] M. Pan, Y. Lu, S. Lu, B. Yu, J. Wei, Y. Liu, Z. Jin, The dual role of bridging phenylene in an extended bipyridine system for high-voltage and stable two-electron storage in redox flow batteries, ACS Appl. Mater. Interfaces. 13 (2021) 44174–44183, https://doi.org/10.1021/acsami.1c09019.
[65] E. Fagadar-Cosma, N. Plesu, A. Lascu, D. Anghel, M. Cazacu, C. Ianasi, G. Fagadar-Cosma, I. Fratilescu, C. Epuran, Novel platinum-porphyrin as sensing compound for efficient fluorescent and electrochemical detection of H2O2, Chemosensors. 8 (2020), https://doi.org/10.3390/CHEMOSENSORS8020029.
[66] K. Peng, Y. Li, G. Tang, Y. Liu, Z. Yang, T. Xu, Solvation regulation to mitigate the decomposition of 2,6-dihydroxyanthraquinone in aqueous organic redox flow batteries, Energy Environ. Sci. 16 (2022) 430–437, https://doi.org/10.1039/d2ee03617g.
[67] J.B. Gerken, C.W. Anson, Y. Preger, P.G. Symons, J.D. Genders, Y. Qiu, W. Li, T. W. Root, S.S. Stahl, Comparison of quinone-based catholytes for aqueous redox flow batteries and demonstration of long-term stability with tetrasubstituted quinones, Adv. Energy Mater. 10 (2020) 1–7, https://doi.org/10.1002/aenm.202000340.
[68] T.T.H. Tran, Y.-R. Chang, T.K.A. Hoang, M.-Y. Kuo, Y.O. Su, Electrochemical behavior of meso -substituted porphyrins: the role of cation radicals to the half-wave oxidation potential splitting, J. Phys. Chem. a. 120 (2016) 5504–5511, https://doi.org/10.1021/acs.jpca.6b03538.
[69] C.C. Fernández, M. Franke, H.P. Steinrück, O. Lytken, F.J. Williams, Demetalation of surface porphyrins at the solid-liquid interface, Langmuir. 37 (2021) 852–857, https://doi.org/10.1021/acs.langmuir.0c03197.
[70] H. Darmokoesoemo, I.K. Murwani, N. Meirmaziza, H. Setyawati, Performance of complex compound Zn-TPP (5,10,15,20-tetrafenylporphyrin) as a dye sensitizer in increasing the current and voltage of dye sensitized solar cells, IOP Conf. Ser. Earth Environ. Sci. 1312 (2024), https://doi.org/10.1088/1755-1315/1312/1/012019.
[71] R. Alexandrova, R. Kalfin, R. Tudose, E. Fagadar-Cosma, Comparative cytotoxicity assays performed using a free porphyrin and its Zn(II), Co(II) and Cu (II) complexes. Influence of optical and aggregation properties, Stud. Univ. Babes-Bolyai Chem. 63 (2018) 65–77, https://doi.org/10.24193/subbchem.2018.4.05.
[72] S. Amanullah, A. Dey, The role of porphyrin peripheral substituents in determining the reactivities of ferrous nitrosyl species, Chem. Sci. 11 (2020) 5909–5921, https://doi.org/10.1039/d0sc01625j.
[73] M. Luciano, C. Brückner, Modifications of porphyrins and hydroporphyrins for their solubilization in aqueous media, 2017. https://doi.org/10.3390/molecules22060980.
[74] T. Shimizu, K. Wakamatsu, Y. Yamada, Y. Toyoda, S. Akine, K. Yoza, H. Yoshikawa, Application of μ-nitrido- And μ-carbido-bridged iron phthalocyanine dimers as cathode-active materials for rechargeable batteries, ACS Appl. Mater. Interfaces. 13 (2021) 40612–40617, https://doi.org/10.1021/acsami.1c10540.
[75] C.H. Chen, C. Liu, B. Liu, The effect of alkoxyl groups on the photoproperties of meta-octasubstituted tetraphenyl porphyrins, Inorg. Chem. Commun. 146 (2022) 110139, https://doi.org/10.1016/j.inoche.2022.110139.
[76] A.K. Paul, S.C. Karunakaran, J. Joseph, D. Ramaiah, Amino acid-porphyrin conjugates: synthesis and study of their photophysical and metal ion recognition properties, Photochem. Photobiol. 91 (2015) 1348–1355, https://doi.org/10.1111/php.12527.
[77] J. Montero, W. da Silva Freitas, B. Mecheri, M. Forchetta, P. Galloni, S. Licoccia, A. D'Epifanio, A neutral-pH aqueous redox flow battery based on sustainable organic electrolytes, ChemElectroChem. 10 (2023) 1–7, https://doi.org/10.1002/celc.202201002.
[78] I.G.B. Maiya, I.C. Araullo, Micellar effects on the aggregation of tetraanionic porphyrins, Spectroscopic Characterization of Free-Base 20 (1989) 2125–2131.
[79] R.A.E. Falvo, L.M. Mink, D.F. Marsh, Microscale synthesis and 1H NMR analysis of tetraphenylporphyrins, J. Chem. Educ. 76 (1999) 237–239, https://doi.org/10.1021/ed076p237.
[80] G. Calogero, A. Bartolotta, G. Di Marco, A. Di Carlo, F. Bonaccorso, Vegetable-based dye-sensitized solar cells, Chem. Soc. Rev. 44 (2015) 3244–3294, https://doi.org/10.1039/c4cs00309h.
[81] D. Dolphin, R.H. Felton, The Biochemical significance of porphyrin .pi. cation radicals, Acc. Chem. Res. 7 (1974) 26–32, https://doi.org/10.1021/ar50073a005.
[82] M. Lovisari, O. Reid Kelly, A.R. McDonald, Hydrocarbon oxidation by a porphyrin-π-cation radical complex, e202303083, Angew. Chemie Int. Ed. 62 (2023), https://doi.org/10.1002/anie.202303083.
[83] H. Yamang, J. Bhuyan, Quest for iron(III) isoporphyrins: synthesis, characterization, reactivity and theoretical studies, J. Mol. Struct. 1296 (2024) 136754, https://doi.org/10.1016/j.molstruc.2023.136754.

[84] X. Wang, L. Zhao, R. Ma, Y. An, L. Shi, Stability enhancement of ZnTPPS in acidic aqueous solutions by polymeric micelles, Chem. Commun. 46 (2010) 6560–6562, https://doi.org/10.1039/c0cc01674h.

[85] M. Zannotti, R. Giovannetti, B. Minofar, D. Řeha, L. Plačková, C.A. D'Amato, E. Rommozzi, H.V. Dudko, N. Kari, M. Minicucci, Aggregation and metal-complexation behaviour of THPP porphyrin in ethanol/water solutions as function of pH, Spectrochim. Acta - Part A Mol, Biomol. Spectrosc. 193 (2018) 235–248, https://doi.org/10.1016/j.saa.2017.12.021.

[86] S.M. Safar Sajadi, S. Khoee, The simultaneous role of porphyrins' H- and J-aggregates and host–guest chemistry on the fabrication of reversible Dextran-PMMA polymersome, Sci. Rep. 11 (2021) 1–14, https://doi.org/10.1038/s41598-021-82256-7.

[87] S. Okada, H. Segawa, Substituent-control exciton in J-aggregates of protonated water-insoluble porphyrins, J. Am. Chem. Soc. 125 (2003) 2792–2796, https://doi.org/10.1021/ja017768j.

[88] M. Neumann-Spallart, K. Kalyanasundaram, On the one and two-electron oxidations of water-soluble zinc porphyrins in aqueous media, zeitschrift fur naturforsch. - sect. B, J. Chem. Sci. 36 (1981) 596–600, https://doi.org/10.1515/znb-1981-0512.

[89] K. Kalyanasundaram, M. Neumann-Spallart, Photophysical and redox properties of water-soluble porphyrins in aqueous media, J. Phys. Chem. 86 (1982) 5163–5169, https://doi.org/10.1021/j100223a022.

[90] M.A. Castriciano, A. Romeo, V. Villari, N. Micali, L. Monsu, S. Sperone, V. S. Agata, Structural Rearrangements in 5,10,15,20-Tetrakis(4-sulfonatophenyl) porphyrin J-aggregates under strongly acidic conditions, J. Phys. Chem. b. 107 (2003) 8765–8771.

[91] A. Zurita, A. Duran, J.M. Ribó, Z. El-Hachemi, J. Crusats, Hyperporphyrin effects extended into a J-aggregate supramolecular structure in water, RSC Adv. 7 (2017) 3353–3357, https://doi.org/10.1039/c6ra27441b.

[92] T. Osakai, K. Muto, Ion transfer and photoinduced electron transfer of water-soluble porphyrin at the nitrobenzene water interface, J. Electroanal. Chem. 496 (2001) 95–102, https://doi.org/10.1016/S0022-0728(00)00356-9.

[93] L. Liu, Y. Li, M. Liu, Acidichromism and supramolecular chirality of tetrakis(4-sulfonatophenyl) porphyrin in organized molecular films, J. Phys. Chem. c. 112 (2008) 4861–4866, https://doi.org/10.1021/jp709734d.

[94] C. He, Q. He, C. Deng, L. Shi, D. Zhu, Y. Fu, H. Cao, J. Cheng, Turn on fluorescence sensing of vapor phase electron donating amines via tetraphenylporphyrin or metallophenylporphrin doped polyfluorene, Chem. Commun. 46 (2010) 7536–7538, https://doi.org/10.1039/c0cc01972k.

[95] X. Feng, Y. Huan, C. Zheng, C. Tan, H. Meng, B. Liu, D. Gao, W. Huang, A series of porphyrins as interfacial materials for inverted perovskite solar cells, Org. Electron. 77 (2020) 105522, https://doi.org/10.1016/j.orgel.2019.105522.

[96] M. Trapani, I.G. Occhiuto, R. Zagami, G. De Luca, M.A. Castriciano, A. Romeo, L. M. Scolaro, R.F. Pasternack, Mechanism for Copper(II)-mediated disaggregation of a porphyrin J-aggregate, ACS Omega. 3 (2018) 18843–18848, https://doi.org/10.1021/acsomega.8b02913.

[97] Y. Li, R.P. Steer, Kinetics of disaggregation of a non-covalent zinc tetraphenylporphyrin dimer in solution, Chem. Phys. Lett. 373 (2003) 94–99, https://doi.org/10.1016/S0009-2614(03)00539-6.

[98] K.M. Kadish, E. Van Caemelbecke, Electrochemistry of porphyrins and related macrocycles, J. Solid State Electrochem. 7 (2003) 254–258, https://doi.org/10.1007/s10008-002-0306-3.

[99] P. Neta, A. Harriman, Zinc porphyrin m-radical cations in aqueous solution, J. Chem. Soc., Farad. Trans. 2 (81) (1985) 123–138.

[100] Y.O. Su, G. Kim, Dongho, Spiro, Isoporphyrin formation upon electrochemical oxidation of zinc tetrakis(4-sulfonato-phenyl)porphine in aqueous solution, J. Electroanal. Chem. 246 (1988) 363–371, https://doi.org/10.1016/0022-0728(88)80172-4.

[101] A. Tang, J. Bao, M. Skyllas-Kazacos, Dynamic modelling of the effects of ion diffusion and side reactions on the capacity loss for vanadium redox flow battery, J. Power Sources. 196 (2011) 10737–10747, https://doi.org/10.1016/j.jpowsour.2011.09.003.

[102] Y. Liu, M.A. Goulet, L. Tong, Y. Liu, Y. Ji, L. Wu, R.G. Gordon, M.J. Aziz, Z. Yang, T. Xu, A long-lifetime all-organic aqueous flow battery utilizing TMAP-TEMPO radical, Chem. 5 (2019) 1861–1870, https://doi.org/10.1016/j.chempr.2019.04.021.

[103] J. Kim, A.J. Bard, Application of the koutecký-levich method to the analysis of steady state voltammograms with ultramicroelectrodes, Anal. Chem. 88 (2016) 1742–1747, https://doi.org/10.1021/acs.analchem.5b03965.

[104] W. da Silva Freitas, A. D'Epifanio, C. Lo Vecchio, I. Gatto, V. Baglio, V.C.A. Ficca, E. Placidi, B. Mecheri, Tailoring MOF structure via iron decoration to enhance ORR in alkaline polymer electrolyte membrane fuel cells, Chem. Eng. J. 465 (2023) 142987, https://doi.org/10.1016/j.cej.2023.142987.

[105] L. Zhang, Y. Qian, R. Feng, Y. Ding, X. Zu, C. Zhang, X. Guo, W. Wang, G. Yu, Reversible redox chemistry in azobenzene-based organic molecules for high-capacity and long-life nonaqueous redox flow batteries, Nat. Commun. 11 (2020) 1–11, https://doi.org/10.1038/s41467-020-17662-y.

[106] C.J. Guo, D. de Kee, Effect of molecular size and free volume on diffusion in liquids, Chem. Eng. Sci. 46 (1991) 2133–2141, https://doi.org/10.1016/0009-2509(91)80171-T.

[107] J. Heinze, Cyclic voltammetry-"electrochemical spectroscopy", Angew. Chemie Int. Ed. English. 23 (1984) 831–847, https://doi.org/10.1002/anie.198408313.

[108] J. Luo, B. Hu, C. Debruler, Y. Bi, Y. Zhao, B. Yuan, M. Hu, W. Wu, T.L. Liu, Unprecedented capacity and stability of ammonium ferrocyanide catholyte in pH neutral aqueous redox flow batteries, Joule. 3 (2019) 149–163, https://doi.org/10.1016/j.joule.2018.10.010.

[109] B. Hu, J. Luo, M. Hu, B. Yuan, T.L. Liu, A pH-neutral, metal-free aqueous organic redox flow battery employing an ammonium anthraquinone anolyte, Angew. Chemie - Int. Ed. 58 (2019) 16629–16636, https://doi.org/10.1002/anie.201907934.

[110] O. Nolte, R. Geitner, I.A. Volodin, P. Rohland, M.D. Hager, U.S. Schubert, State of charge and state of health assessment of viologens in aqueous-organic redox-flow electrolytes using in situ IR spectroscopy and multivariate curve resolution, Adv. Sci. 9 (2022) 1–10, https://doi.org/10.1002/advs.202200535.

[111] A. Trabolsi, N. Khashab, A.C. Fahrenbach, D.C. Friedman, M.T. Colvin, K.K. Cotí, D. Benítez, E. Tkatchouk, J.C. Olsen, M.E. Belowich, R. Carmielli, H.A. Khatib, W. A. Goddard, M.R. Wasielewski, J.F. Stoddart, Radically enhanced molecular recognition, Nat. Chem. 2 (2010) 42–49, https://doi.org/10.1038/nchem.479.

[112] T.M. Bockman, J.K. Kochi, Isolation and Oxidation-Reduction of Methylviologen Cation Radicals. Novel Disproportionation in Charge-Transfer Salts by X-ray crystallography, J. Org. Chem. 55 (1990) 4127–4135, https://doi.org/10.1021/jo00300a033.

[113] K.E. Preuss, Pancake bonds: π-Stacked dimers of organic and light-Atom radicals, Polyhedron. 79 (2014) 1–15, https://doi.org/10.1016/j.poly.2014.04.005.

[114] C. Debruler, B. Hu, J. Moss, J. Luo, T.L. Liu, A sulfonate-functionalized viologen enabling neutral cation exchange aqueous organic redox flow batteries toward renewable energy storage, ACS Energy Lett. 3 (2018) 663–668, https://doi.org/10.1021/acsenergylett.7b01302.

[115] J. Haumesser, J.P. Gisselbrecht, L. Karmazin-Brelot, C. Bailly, J. Weiss, R. Ruppert, Synthesis and electrochemical studies of porphyrin dimers linked by metallocarbenes, Organometallics. 33 (2014) 4923–4930, https://doi.org/10.1021/om5002099.

[116] E. Ojadi, R. Selzer, H. Linschitz, Properties of porphyrin dimers, formed by pairing cationic and anionic porphyrins, 107 (1985) 7783–7784.

[117] C.-N. Sun, F.M. Delnick, D.S. Aaron, A.B. Papandrew, M.M. Mench, T. A. Zawodzinski, Resolving losses at the negative electrode in all-vanadium redox flow batteries using electrochemical impedance spectroscopy, J. Electrochem. Soc. 161 (2014) A981–A988, https://doi.org/10.1149/2.045406jes.

[118] C.N. Sun, F.M. Delnick, D.S. Aaron, A.B. Papandrew, M.M. Mench, T. A. Zawodzinski, Probing electrode losses in all-vanadium redox flow batteries with impedance spectroscopy, ECS Electrochem. Lett. 2 (2013) 43–46, https://doi.org/10.1149/2.001305eel.

[119] P. Leuaa, D. Priyadarshani, D. Choudhury, R. Maurya, M. Neergat, Resolving charge-transfer and mass-transfer processes of VO2+/VO2 + redox species across the electrode/electrolyte interface using electrochemical impedance spectroscopy for vanadium redox flow battery, RSC Adv. 10 (2020) 30887–30895, https://doi.org/10.1039/d0ra05224h.

[120] J. Chai, X. Wang, A. Lashgari, C.K. Williams, J. "Jimmy" Jiang, A pH-neutral, aqueous redox flow battery with a 3600- cycle lifetime: micellization-enabled high stability and crossover suppression, ChemSusChem. 13 (2020) 4069–4077, https://doi.org/10.1002/cssc.202001286.